Measurement of Critical Contact Angle
in a Microgravity Space Experiment

P. Concus, R. Finn, M. Weislogel

Abstract Mathematical theory predicts that small changes in container shape or in contact angle can give rise to large shifts of liquid in a microgravity environment. This phenomenon was investigated in the Interface Configuration Experiment on board the USML-2 Space Shuttle flight. The experiment's "double proboscis" containers were designed to strike a balance between conflicting requirements of sizable volume of liquid shift (for ease of observation) and abruptness of the shift (for accurate determination of critical contact angle). The experimental results support the classical concept of macroscopic contact angle and demonstrate the role of hysteresis in impeding orientation toward equilibrium.

1. Introduction

When planning space-based operations, it is important to be able to predict the equilibrium locations and configurations that fluids will assume in containers under low-gravity conditions. Currently available mathematical theory applies completely, however, to only a few particular configurations, such as the partially filled right circular cylindrical container with liquid simply covering the base. Behavior in space for such a configuration, although different from what is familiar in common experience with a terrestrial environment, is at least consistent with that experience. For more general containers, however, fluids in reduced gravity can behave in striking, unexpected ways.

P. Concus, Lawrence Berkeley Laboratory and Department of Mathematics, University of California, Berkeley, CA 94720 (to whom correspondence should be addressed)
R. Finn, Department of Mathematics, Stanford University, Stanford, CA 94305
M. Weislogel, NASA Lewis Research Center, Cleveland, OH 44135

The classical theory, according to the Young-Laplace-Gauss (Y-L-G) formulation, characterizes fluid locations as equilibrium configurations for the surface-plus-gravitational mechanical energy. Using this point of view in a mathematical study, we have shown that for a cylindrical container of general cross-section in zero gravity the surface change arising from small changes in geometry or contact angle can be discontinuous or "nearly discontinuous," leading to large shifts of the liquid mass. Attempts to observe this behavior experimentally can be valuable as tests of validity of the concept of macroscopic contact angle used in the classical theory, and thereby of the theory's effectiveness in predicting fluid behavior.

The principal mathematical result underlying the behavior is that for particular cylindrical sections a discontinuous kind of change can be realized as the contact angle γ crosses a critical value γ_0 intrinsic to the container. (In this paper we shall restrict subsequent discussion, without loss of generality, to be in terms of a partially wetting liquid ($0 < \gamma < \pi/2$), which is the case for the materials used in the space experiment.) When γ is larger than γ_0 there exists an equilibrium configuration of liquid that covers the base of the cylindrical container simply, while for contact angles smaller than γ_0 no such equilibrium configuration is possible. In the latter case liquid moves to the walls and can rise arbitrarily high along a part of the wall, uncovering a portion of the base if the container is tall enough. By simple physical observation of bulk behavior of the liquid, one can thereby determine whether the contact angle is larger than or smaller than the critical value for the container. A practical challenge in this connection is to design cross-sections for which a large enough portion of the liquid will rise up the walls for ease of observation as the critical value of contact angle is crossed, without the containers being unrealistically tall, and so that the change will be abrupt enough to allow accurate determination of critical contact angle value.

By using two or more containers corresponding to appropriately chosen values of γ_0, differing, say, by the accuracy desired for contact angle evaluation, one can determine the value of the critical contact angle to lie within a particular interval. In some cases, ge-

ometries can be "combined" into a single container for determining such an interval. For our Interface Configuration Experiment (ICE) on the second United States Microgravity Laboratory (USML-2) Space Shuttle flight STS-73 these two approaches were conjoined.

The experiment was conducted in the Glovebox, a multi-user facility developed by the European Space Agency/ESTEC, Brunel Institute for Bioengineering (United Kingdom), and Bradford Engineering (The Netherlands) for experiments on Spacelab missions or in the Shuttle middeck. Originally designed to handle biological experiments, the Glovebox has been adapted to handle fluids, combustion, and material science experiments and has served well as a rapid and inexpensive platform in which to conduct experiments in space. ICE utilized the Glovebox primarily as a staging area and a level of containment in the event of a fluid spill.

Mathematical and computational results that form the basis for ICE, as well as results of pre-flight drop tower experiments, are described in Chen et al. (1997). Some of these results are included here for convenience, primarily in Sec. 2 and the figures therein. Further mathematical background and historical information are given by Finn (1986) and by Concus and Finn (1974, 1990). Some related work is described by Langbein (1990, 1995) and by Langbein et al. (1990). In addition to the containers reported here, ICE included also a movable wedge container, the results for which we plan to discuss in a separate study.

2. Mathematical and Computational Background

2.1 Canonical Proboscis Containers

The "double proboscis" containers used in the USML-2 experiment derive from the "canonical proboscis" containers introduced by Fischer and Finn (1993). These, in turn, can be thought of as generalizations of a basic wedge container (Fig. 1), a cylindrical container whose section Ω consists of a circular arc and a smoothly joined protruding corner of

interior angle 2α. For the wedge container the transition at the critical contact angle $\gamma_0 = \pi/2 - \alpha$ is sharp. For $\gamma_0 \leq \gamma < \frac{\pi}{2}$ and for liquid volume sufficient to cover the base, the height of the free surface S can be given in closed form as a portion of a lower hemisphere meeting the walls with the prescribed contact angle γ. Thus for given volume of liquid the height is bounded uniformly in γ throughout this range. For $0 \leq \gamma < \gamma_0$, the liquid will move to the corner and rise arbitrarily high at the vertex P, uncovering the base regardless of liquid volume. The behavior for the wedge domain is thus discontinuous at $\gamma = \gamma_0$. Physical procedures for determining critical contact angle in this container can give very good accuracy for larger values of γ (closer to $\pi/2$) but may be subject to experimental inaccuracy when γ is closer to zero, as the part of the section over which the liquid accumulates when the critical angle γ_0 is crossed then becomes very small and may be difficult to observe.

The canonical proboscis containers provide a way of overcoming the above experimental difficulty. These containers are cylinders whose cross-sections consist of a circular arc attached symmetrically to a (symmetric) pair of curves described by

$$x + C = \sqrt{{R_0}^2 - y^2} + R_0 \sin\gamma_0 \ \ln \frac{\sqrt{{R_0}^2 - y^2}\cos\gamma_0 - y\sin\gamma_0}{R_0 + y\cos\gamma_0 + \sqrt{{R_0}^2 - y^2}\ \sin\gamma_0} \qquad (1)$$

and meeting at a point P on the x-axis, see Fig. 2. Here R_0, as well as the particular points of attachment, may be chosen arbitrarily. The continuum of circular arcs Γ_0, of which three are depicted by the dashed curves in Fig. 2, are horizontal translates of one such arc, of radius R_0 and with center on the x-axis, and the curves (1) have the property that they meet all the arcs Γ_0 in the constant angle γ_0. The radius ρ of the circular boundary arc can be chosen in such a way that γ_0 becomes the critical contact angle value for the container. Specifically, one can show mathematically that a solution of the Y-L-G equations governing the equilibrium liquid free-surface can exist in Ω if and only if $\gamma > \gamma_0$ and that the liquid height rises unboundedly as γ decreases to γ_0, precisely in the region swept out by the arcs Γ_0 (the entire proboscis region to the right of the leftmost arc Γ_0 shown in Fig. 2). Furthermore a unique value of ρ can be obtained for any prescribed

proboscis length, and there holds $R_0 \cos\gamma_0 < \rho < 2R_0$. Thus, the behavior is not strictly discontinuous as for the basic planar wedge container—the liquid shifts increasingly toward the proboscis wall as γ decreases to γ_0—but it can be "nearly discontinuous".

Numerical solutions depicting such behavior are given by Concus et al. (1992) for some canonical proboscis containers. For these containers the rise height in the proboscis can be relatively modest until γ decreases to values close to γ_0, and then becomes very rapid as γ decreases still further. Since the proboscis can be made relatively as large a portion of the section as desired, the shift can be easily observed for a broad range of γ_0. Through proper choice of the domain parameters for the cases considered, an effective balance can be obtained between conflicting requirements of a sharp near discontinuity (for accurate measurement) and a sizable volume of liquid rise (for ease of observation).

2.2 Double Proboscis Containers

The double proboscis containers for ICE are similar to the single proboscis one of Fig. 2, except that there is a second proboscis diametrically opposite to the first, in effect combining two single proboscis containers into one. The values of γ_0 in (1) differ for the left and right proboscides, whose values of γ_0 we denote by γ_L and γ_R, respectively. Similarly, we denote the values of R_0 for the left and right proboscides by R_L and R_R. These satisfy $R_R \cos\gamma_R = R_L \cos\gamma_L$. The critical value for the container is the larger of γ_L and γ_R. For the discussion here, we shall take $\gamma_R > \gamma_L$, so that the critical contact angle γ_0 for a container is equal to γ_R.

The container cross-sections for the experiment, superimposed on one another, are shown in Fig. 3. They have been scaled so that the circular portions all have radius unity. The meeting points of the vertices with the x-axis are, respectively, a distance 1.5 and 1.6 from the circle center. For the sections depicted in Fig. 3 the values of γ_L and γ_R are respectively 20° and 26° for the outermost section, 30° and 34° for the middle section, and 38° and 44° for the innermost section.

For these containers the explicit behavior has not been determined mathematically in the complete detail that it has for the single proboscis containers. However, numerical computations and the known behavior of the single proboscis solution surfaces indicate a predicted behavior as follows: For contact angles $\gamma \geq \gamma_0$, as γ decreases to γ_0 the liquid will rise higher in the right than in the left proboscis, with the rise becoming unbounded in the right proboscis at γ_0. For contact angles between γ_L and γ_R the liquid will rise arbitrarily high in the right proboscis, but the height in the left will still be bounded. For smaller contact angles the liquid will rise up both proboscides arbitrarily high. By observing the liquid shift, one can then bracket the contact angle relative to the values of γ_L and γ_R. For a practical situation in which the container is of finite height with a lid on the top, the liquid will rise to the lid along one or both of the proboscides in the manner described above (provided the liquid volume is adequate); in some cases, liquid may then travel along the corner at the lid and flow into the other proboscis from the top.

The selected values of γ_L and γ_R for the three containers are based on the value of approximately 32° measured in a terrestrial environment for the contact angle between the ICE experiment liquid and the acrylic plastic material of the container. The spread of values of contact angle covered by the three containers is intended to allow observation of possible effects of contact angle hysteresis, which is not included in the classical theory.

2.3 Computed Surfaces

The mathematical equations governing the free surface were solved numerically for the three double proboscis container sections depicted in Fig. 3, for a range of contact angles γ, to obtain details of the anticipated liquid behavior. It was adequate to compute solutions for the upper-half domains only, because of the reflective symmetry. The adaptive-grid finite-element software package PLTMG of Bank (1994) was used.

The numerically calculated solution surface for the upper half of the 30°/34° domain is shown in Fig. 4 for four values of contact angle, 60°, 50°, 40°, and 35°. (The critical

value for the domain is $\gamma_0 = 34°$.) The three-dimensional views of the surface are color-shaded by PLTMG to indicate contour levels, The viewpoint for each surface is the same. Generally, the computations indicate that as γ decreases toward the critical contact angle, liquid moves toward and up the two proboscis walls, with the local maximum heights, as calculated by the program, at the proboscis tips. The heights at the right are higher than the corresponding ones at the left. The surfaces for the 20°/26° and 36°/44° proboscis domains behave similarly.

One sees that the numerically computed rise height in the container is modest until γ gets close to the critical value. The computations indicate that using containers of sufficient height (five for our containers), one could distinguish between the critical value γ_0 for the container (liquid in right proboscis rises to the lid) and a contact angle value one degree greater (liquid rise height less than five).

3. Experiment Results

All double proboscis vessels flown were similar in construction; the 38°/44° vessel is depicted in Fig. 5. The primary vessel components are a two-piece acrylic-plastic (transparent) body, an aluminum piston and control dial, a stainless steel drive screw, an aluminum valve, and an aluminum base for securing the vessel to the experiment platform. O-ring seals are employed throughout. The internal surfaces of the proboscis vessels were precision milled on a numerically-controlled machine using a diamond tipped cutting tool; the coordinates were computed from (1). The critical surfaces were finished by an extremely light polish ("wipe") using a dry cloth. These vessels were fabricated in halves divided by the plane of symmetry, and the two halves were fused without corruption of the interior corner at the joint. Post-fabrication calibration of the vessels revealed a mean tolerance of less than 76μm for the proboscis shapes, as determined by the distance of the container wall to the measured cylinder axis. Based on the maximum container dimension of 1.5cm, compliance of the proboscis profiles with those determined mathematically were estimated to be within $\pm 0.5\%$.

The general experimental procedure for ICE during the USML-2 flight was to partially fill the selected vessels with prescribed volumes of fluid and to record with video cameras the fluid interface configurations that resulted. The crew procedures for carrying out the experiment consisted primarily of the steps: (1) unstow equipment, (2) set up Glovebox and vessel, (3) charge vessel/activate, (4) observe stable surfaces, (5) disturb surface configuration(s), (6) observe resulting surfaces, (7) repeat (5) and (6), and (8) reverse fill procedure and stow. For the three vessels a total of approximately ninety minutes were required. The Spacelab Camcorder and a Glovebox full-color 1:1 video camera were utilized. Devices for the measurement of ambient Glovebox temperature and local acceleration levels were also used. Fig. 6 shows crew member Fred Leslie conducting the experiment in the Spacelab Glovebox during the mission.

To begin the experiment, a crew member retrieves the Spacelab Camcorder (Hi-8mm format) and unstows the ICE vessel to be tested. A diffuse backlight panel provided illumination for the video photography.

The test liquid for all the double proboscis vessels was an aqueous ethanol solution, 50% by volume. This particular concentration was selected for the specific wetting conditions desired. A red dye was added to enhance observations. The longtime "equilibrium" contact angle for this liquid mixture on acrylic plastic in the presence of ethanol saturated air was measured by the sessile drop method to be $32° \pm 2°$. The largest range of static contact angle hysteresis measured for the liquid on a machined, lightly-polished acrylic surface was 18° for the receding value and 43° for the advancing value by the tilt-slide method. Mean values were 20° and 41°, respectively, with an equilibrium value of $\gamma_{eq} = 32°$, all values producing a consistent uncertainty of $\pm 2°$. The density, kinematic viscosity, and surface tension for the dyed aqueous ethanol solution were measured to be $\rho_0 = 896 \text{kg/m}^3$, $\nu = 2.75 \times 10^{-6} \text{m}^2/\text{s}$, and $\sigma = 0.0308 \text{N/m}$, respectively.

To carry out the fill procedure, the crew member pulled open the reservoir valve and turned the control dial, displacing the entire liquid contents of the reservoir into the double proboscis container (cf., Fig. 5). The liquid then assumed a particular "static" configuration

(not necessarily an equilibrium configuration. A static configuration of an interface implies a possibly metastable state, common in partially wetting, contact-line-dominated situations exhibiting significant contact angle hysteresis, see Kistler (1993, p. 328)). Time was allowed for the configuration to stabilize (up to 5 min). The crew member then disturbed the surface by tapping the side of the container with his finger, lightly at first and then subsequently with increasing force. All new surfaces that formed in the container during the tapping process were given time to stabilize and were captured on video. The tapping, which led eventually to larger scale rocking and sloshing, produced different results for each of the three containers. These results are discussed below.

3.1 Vessel ICE-P1

The first vessel tested was ICE-P1, the 20°/26° vessel as depicted in Fig. 3. Both proboscides for this vessel are subcritical for the $\gamma_{eq} = 32°$ liquid. Fig. 7 shows two static interface shapes for the vessel: Fig. 7a was taken shortly after the fill procedure was completed, and Fig. 7b was taken after significant disturbances to the vessel had been imparted by the payload specialist. Very little change in the interface can be distinguished between initial and final states, even though significant disturbances were imparted. This is in accord with the mathematical predictions, as the measured equilibrium contact angle $32° \pm 2°$ is greater than the critical angles for both proboscides. A somewhat elevated surface in the righthand 26° proboscis is anticipated, relative to the lefthand one, as its critical angle is closer to the value $\gamma_{eq} = 32°$ (cf., Fig. 4). Imparting larger disturbances might possibly have "released" the liquid to end up with a somewhat larger height difference between the two probscides, as in, say, the 40° case in Fig. 4, but, generally, the video indicated much more stable behavior for this vessel than for the subsequent ones described below. For vessel P1, and also for vessels P2 and P3, the initial static interface shapes prior to the initiation of disturbances were observed to be largely the same as the terminal ones observed in the pre-flight drop tower tests reported in Chen et al. (1997).

3.2 Vessel ICE-P2

The lefthand/righthand proboscides for this vessel are the 30°/34° ones, so that the lefthand proboscis is subcritical with respect to $\gamma_{eq} = 32°$, while the righthand one is supercritical. A series of static interfaces formed during the test sequence is shown in Fig. 8. Fig. 8a is taken shortly after completion of the fill procedure. Figs. 8b, 8c, and 8d are images of static interface configurations after successive disturbances to the vessel by the payload specialist. For this test, once the liquid fill was completed, light taps on the side of the container produced small, high frequency surface waves, but did not lead to observable bulk reorientation of the liquid. As the disturbances were increased in magnitude, however, instead of returning to the initial state of Fig. 8a (as was the case for vessel ICE-P1 in Fig. 7) the liquid rose noticeably and somewhat equally in the proboscides (Fig. 8b). After allowing sufficient time for stabilization, the crew member repeated the disturbances to the vessel, but not increasing them in magnitude. Each disturbance was imparted by a single "push" (impulse) to the top lefthand side of the vessel which acted to rock the interface with a mean amplitude A of approximately 4mm over a 0.4s interval t_d. Thus, a mean dynamic Bond number $Bo \equiv \rho_0 a R^2/\sigma \doteq 0.33$ may be computed, where a is the effective acceleration of the disturbance ($a \doteq 2A/t_d^2$ assumed constant), R is a characteristic dimension of the container, in this case the radial distance to the vertex of the proboscides ($\doteq$ 0.015m), and ρ_0 and σ are respectively the density and surface tension of the liquid. The interface responded to the impulse disturbance with approximately 1.3Hz damped oscillations that decayed within 10s. The interface was allowed time to stabilize between each disturbance.

As seen in Figs. 8c and 8d, subsequent, larger disturbances, carried out to explore further the initial liquid rise, led to an increased rise only in the 34° righthand supercritical proboscis. The penetration of the liquid into the righthand proboscis took place regardless of whether the disturbances to the cell were applied to the top righthand *or* lefthand side of the vessel. This result indicates, somewhat dramatically, that the slight differences in proboscis fabrication, which were designed to produce unbounded flow up the righthand

proboscis only, do influence fluid behavior strongly, even in the presence of hysteresis. In practice, however, significant disturbances ($\approx 0.05\text{m/s}^2$, $Bo \doteq 0.3$) were necessary in order to overcome contact angle hysteresis and bring about the large shifts of liquid depicted in Figs. 8c–d. (Remark: When $Bo \gtrsim 1$, destabilization and break-up of the surface can be anticipated experimentally, as described by Masica et al. (1964). For the inverted circular cylinder, numerical studies by Concus (1968) indicate similar stability limits.) It is astonishing that though the hysteresis range for the test liquid is $20° \leq \gamma \leq 41°$, the interface behaved in a manner that is in accord with the mathematical predictions based on the idealized Y-L-G theory using a value $\gamma_{eq} = 32°$. It is also striking that the uncertainty of $\pm 2°$ for γ_{eq} did not mask the effect of the subtle differences in the left and right proboscides designed for the 30°/34° critical angles.

3.3 Vessel ICE-P3

Both proboscides for the third vessel, the 38°/44° one, are supercritical for the test fluid. Therefore, the mathematical predictions are that the liquid should rise spontaneously to the lid in both left and right proboscides. Because the right proboscis is more supercritical than the left, greater/faster rise may be anticipated there. A series of images, similar to those in Figs. 8a–d, are presented for vessel ICE-P3 in Fig. 9. Fig. 9a shows the interface after completion of the fill procedure, and Figs. 9b, 9c, and 9d show interfaces after subsequent disturbances to the vessel. Again, each image displays the liquid in a static state. Disturbances to this vessel caused large shifts of the liquid up both proboscides, with more up the righthand proboscis. The liquid continued to penetrate higher in each proboscis regardless of the direction of the impulse disturbance. These results are in accordance with the predictions, except that the liquid did not move spontaneously—significant disturbances ($Bo \lesssim 0.3$) were necessary to bring about equilibrium-type behavior within the approximately 20 minutes allowed for the experiment.

After completion of the ICE-P3 procedures (Fig. 9d), the crew placed the vessel (delicately) in the aft end cone of the Spacelab module, where it was allowed to remain for seven days.

During this time it was observed that the liquid continued to creep, though very slowly, toward the end state configuration of Fig. 10, which was photographed with a 35mm camera at the end of the seven days. The lighting is not as favorable here, but the liquid free surface can still be easily identified. The liquid is seen to have risen further in the lefthand proboscis (cf., Fig. 9d), while the liquid in the righthand proboscis rose to the lid, covered it, at least partially, and then started advancing down the lefthand proboscis. The Y-L-G equilibrium state requires that the base, lid, and entire length of both proboscides be wet by the liquid. (The isolated drop in the lower left quadrant of Fig. 10 was present prior to the long term storage (see Fig. 9d).)

These findings suggest that the theory can indeed be successful in predicting fluid behavior, if sufficient time is available to establish equilibrium. The time required to reach the configuration in Fig. 10 may have been lessened by existing mechanical and thermal disturbances, the latter hastening migration of the liquid toward equilibrium through successive evaporation and condensation, a process (associated with Kelvin energy) not included in the Y-L-G theory. Figs. 9d and 10 show that the fluid bulk remained connected and that condensate drops on the container walls, common in many partial wetting systems subject to temperature cycling on Earth, were not present. We note that liquid near the proboscis tip in the cases for which the theory predicts the liquid still should be advancing (right proboscis in Figs. 8c–d, both proboscides in Figs. 9c–d), resembles the convex shape computed by Weislogel and Lichter (1997) for the tip of a spreading liquid drop in a wedge.

The above results provide insight into the role of container geometry, contact angle, contact angle hysteresis, input disturbances, and length of time in predicting interface configurations. What is clearly established is the role of hysteresis near critical values for which slight changes in container geometry result in large changes in interface configuration. *Hysteresis is found not to prevent the predicted behavior, but only to noticeably impede it.* Significant perturbations to the interface are necessary to "encourage" the fluid to behave as predicted in reasonably rapid time.

4 Conclusions

The USML-2 ICE experiment shows in a striking way the discontinuous type of behavior for the double proboscis containers at the predicted critical angles. Even though hysteresis was large and surface friction impeded reorientation of the liquid, the mathematically predicted behavior at critical contact angle was observed. This lends credence to the validity of the concept of macroscopic contact angle and its Y-L-G formulation as tools for predicting fluid behavior.

Acknowledgments

We wish to thank Fred Leslie for the highly skilled manner in which the experiments reported here were carried out. This work was supported in part by the National Aeronautics and Space Administration under Grants NCC3-329 and NAG3-1941 and by the National Science Foundation under Grants DMS-9400778 and DMS-9401167, and by the Mathematical Sciences Subprogram of the Office of Energy Research, U. S. Department of Energy, under Contract Number DE-AC03-76SF00098.

References

Bank RE (1994) PLTMG: A Software Package for Solving Elliptic Partial Differential Equations, SIAM, Philadelphia; software available via Netlib (WWW: `http://www.netlib.org`, E-mail:`netlib@research.att.com`)

Chen A; Concus P; Finn R; Weislogel M (1997) On cylindrical container sections for a capillary free-surface experiment, Microgravity Sci Technol IX/3:169–174

Concus P (1968) Static Menisci in a Vertical Right Circular Cylinder, J Fluid Mech 34:481–495

Concus P; Finn R (1974) On capillary free surfaces in the absence of gravity, Acta Math 132:177–198

Concus P; Finn R (1990) Dichotomous behavior of capillary surfaces in zero gravity, Microgravity Sci Technol 3:87–92; Errata, 3:230 (1991)

Concus P; Finn R; Zabihi F (1992) On canonical cylinder sections for accurate determination of contact angle in microgravity, in Fluid Mechanics Phenomena in Microgravity, eds. DA Siginer and MM Weislogel, AMD Vol 154, Amer Soc Mech Engineers, New York, pp. 125–131

Finn R (1986) Equilibrium Capillary Surfaces, Springer-Verlag, New York. Russian translation, with Appendix by HC Wente, Mir Publishers (1988)

Fischer B; Finn R (1993) Non-existence theorems and measurement of capillary contact angle, Zeit Anal Anwend 12:405–423.

Kistler SF (1993) in Wettability, ed. JC Berg, Surfactant Science Series 49 Chap 6

Langbein D (1990) The shape and stability of liquid menisci at solid edges, J Fluid Mech 213:251–265

Langbein D (1995) Liquid surfaces in polyhedral containers, in Advances in Geometric Analysis and Continuum Mechanics, eds. P Concus and K Lancaster, International Press, Boston, pp. 175–180

Langbein D; Großbach R; Heide W (1990) Parabolic flight experiments on fluid surfaces and wetting, Microgravity Sci Technol 2:198–211

Masica WJ; Derdul JD; Petrash DA (1964) Hydrostatic Stability of the Liquid-Vapor Interface in a Low-Acceleration Field, NASA TN D-2444.

Weislogel MM; Lichter S (1997) A Spreading Drop in an Interior Corner: Theory and Experiment, Microgravity Sci Technol IX/3:175–184

Figure Captions

Fig. 1. Wedge container.

Fig. 2. Proboscis container section showing three members of the continuum of extremal arcs.

Fig. 3. Three superimposed double proboscis container sections. From outermost to innermost, the pair of values of γ_0 for the left and right proboscides of each section are 20°/26°, 30°/34°, and 38°/44°.

Fig. 4. Computed equilibrium interface for the 30°/34° (upper-half) double proboscis section for contact angles 60°, 50°, 40°, and 35°. $\gamma_0 = 34°$.

Fig. 5. 38°/44° proboscis vessel (flight unit, ICE-P3): 1 proboscis container, 2 control dial, 3 piston/plunger, 4 reservoir valve, 5 fill passage.

Fig. 6. Payload Specialist Fred Leslie conducting ICE-P2 test in Spacelab Glovebox facility: 1 video monitor, 2 Glovebox, 3 proboscis vessel, 4 Spacelab camcorder.

Fig. 7. Static interface shapes for ICE-P1 (20°/26°) vessel. 7a (left): after completion of fill; 7b (right): after disturbances by payload specialist.

Fig. 8. Static interface shapes for ICE-P2 (30°/34°) vessel. 8a (upper left): after completion of fill; 8b (upper right), 8c (lower left), and 8d (lower right): after successive disturbances by payload specialist.

Fig. 9. Static interface shapes for ICE-P3 (38°/44°) vessel. 9a (upper left): after completion of fill; 9b (upper right), 9c (lower left), and 9d (lower right) after successive disturbances by payload specialist.

Fig. 10. Static interface shape for ICE-P3 (38°/44°) vessel one week after that shown in Fig. 9d.

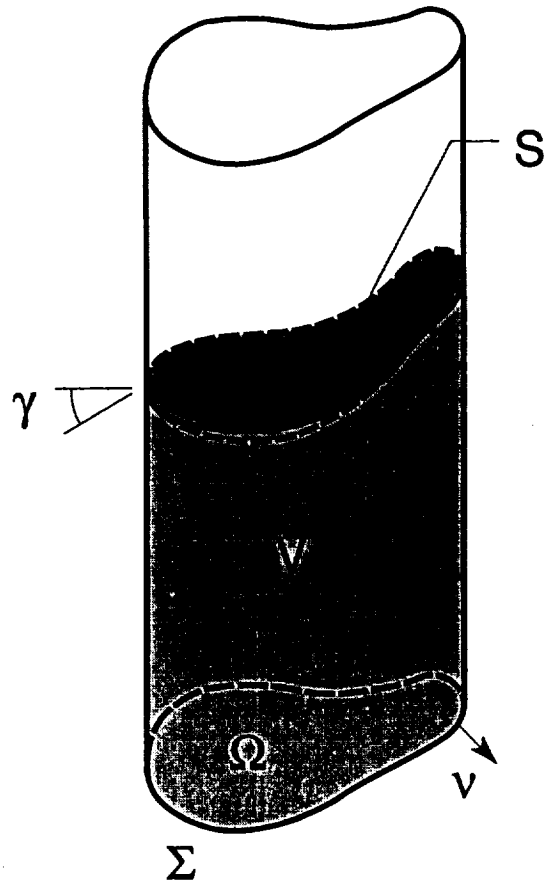

Fig. 1.

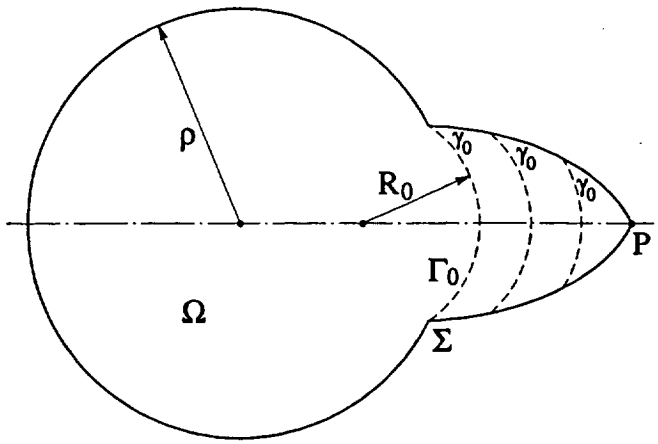

Fig 2.

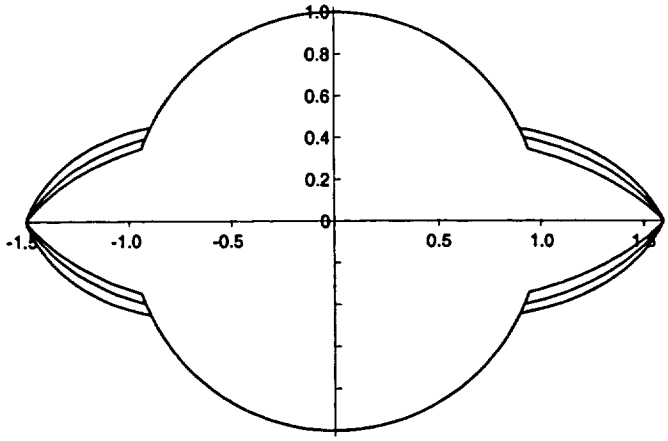

Fig. 3.

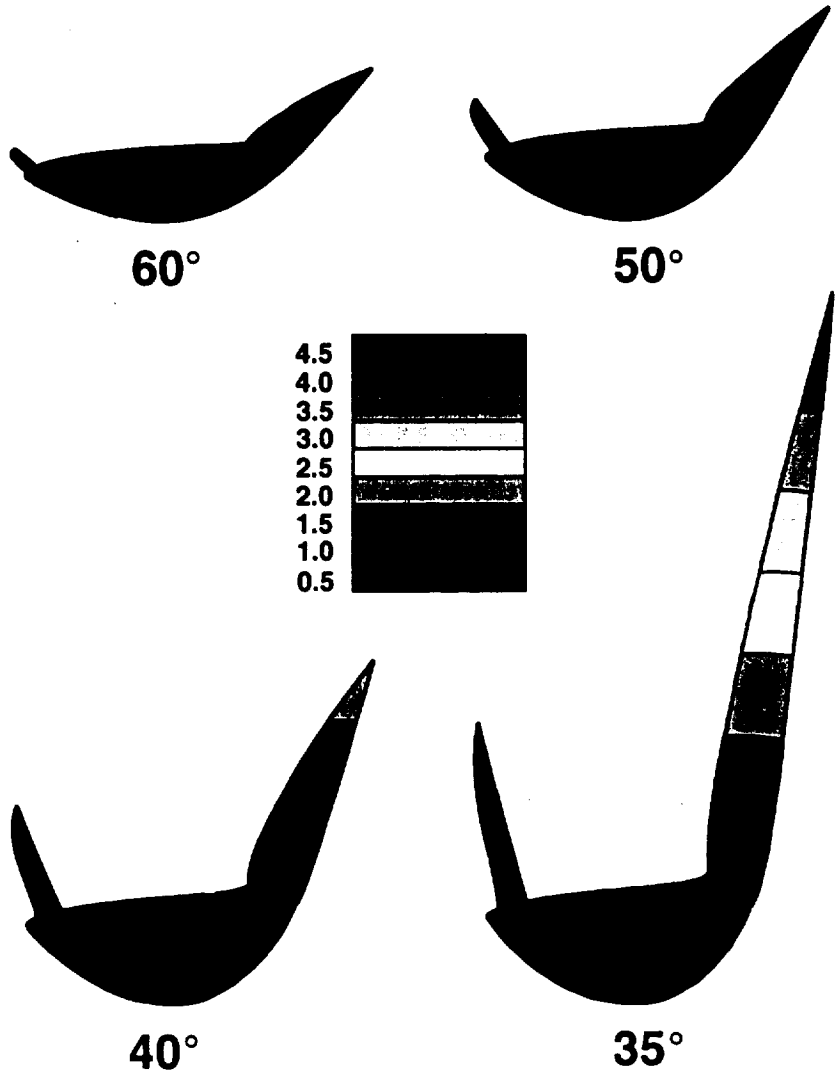

Fig 4

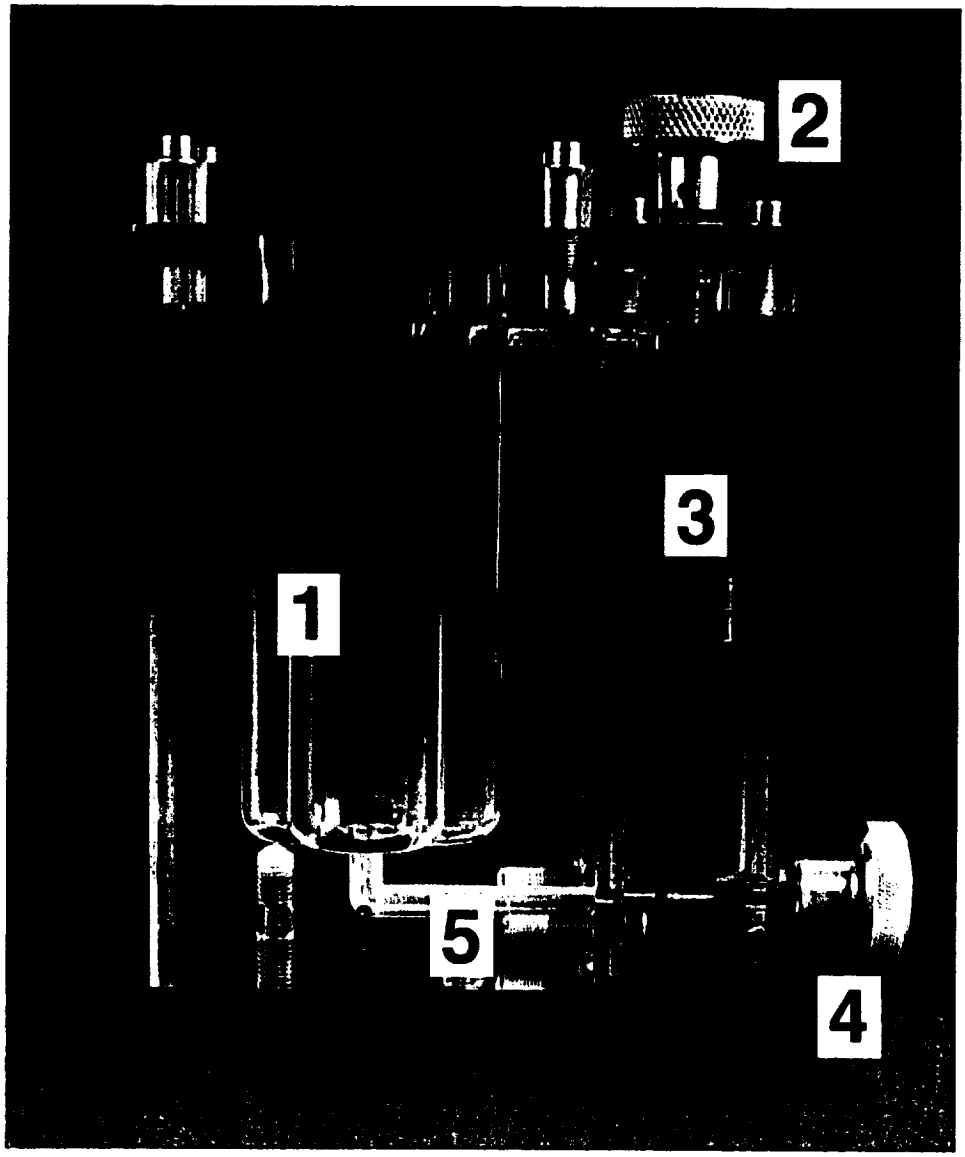

Fig 5

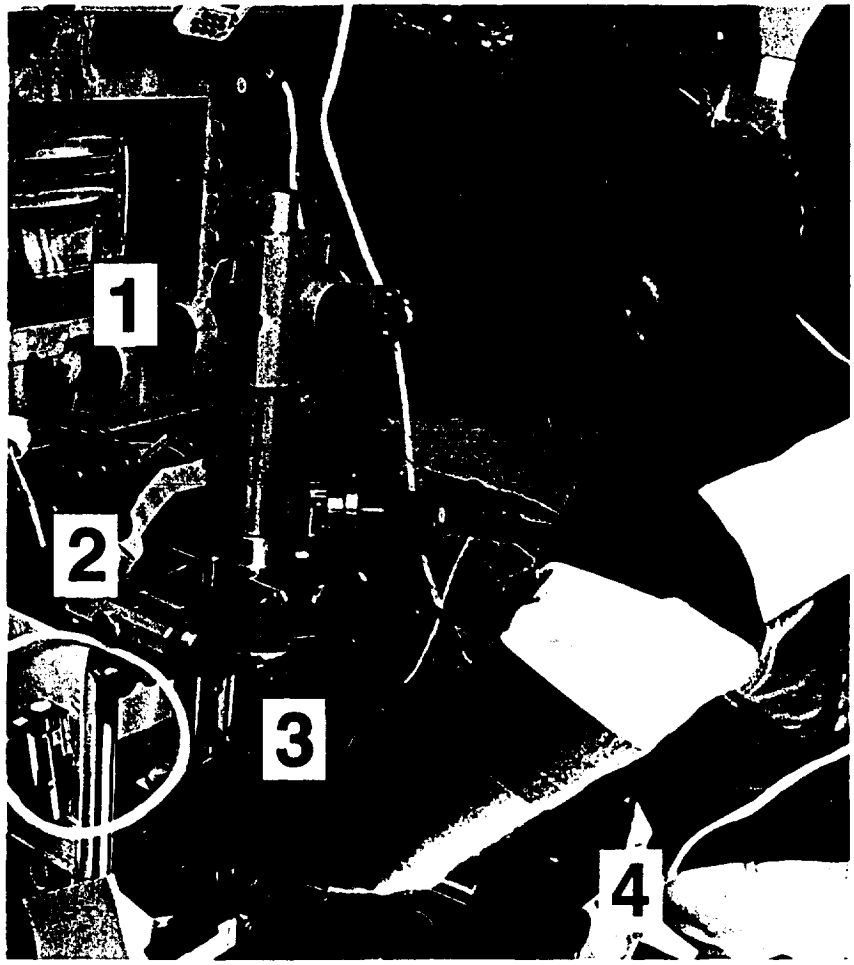

Fig 6

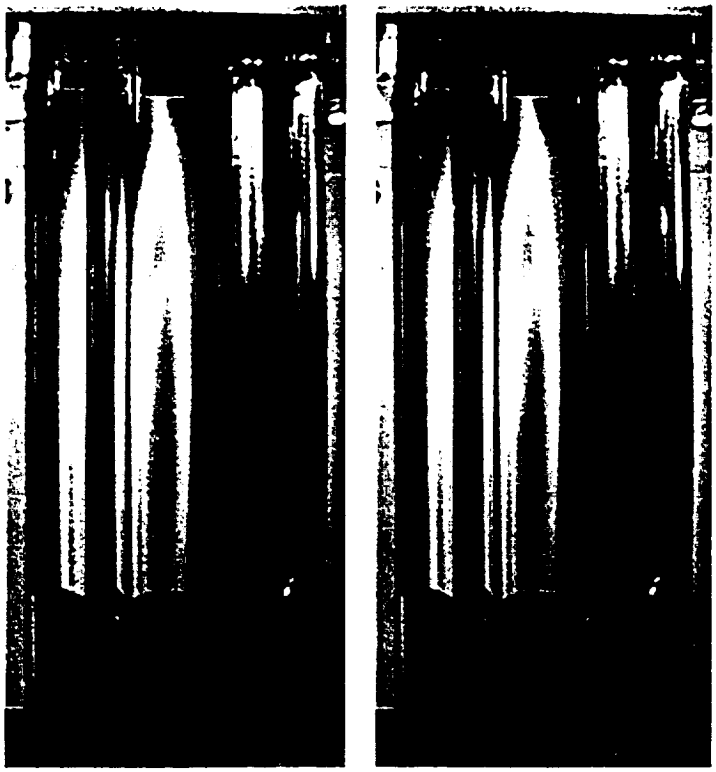

Fig 7

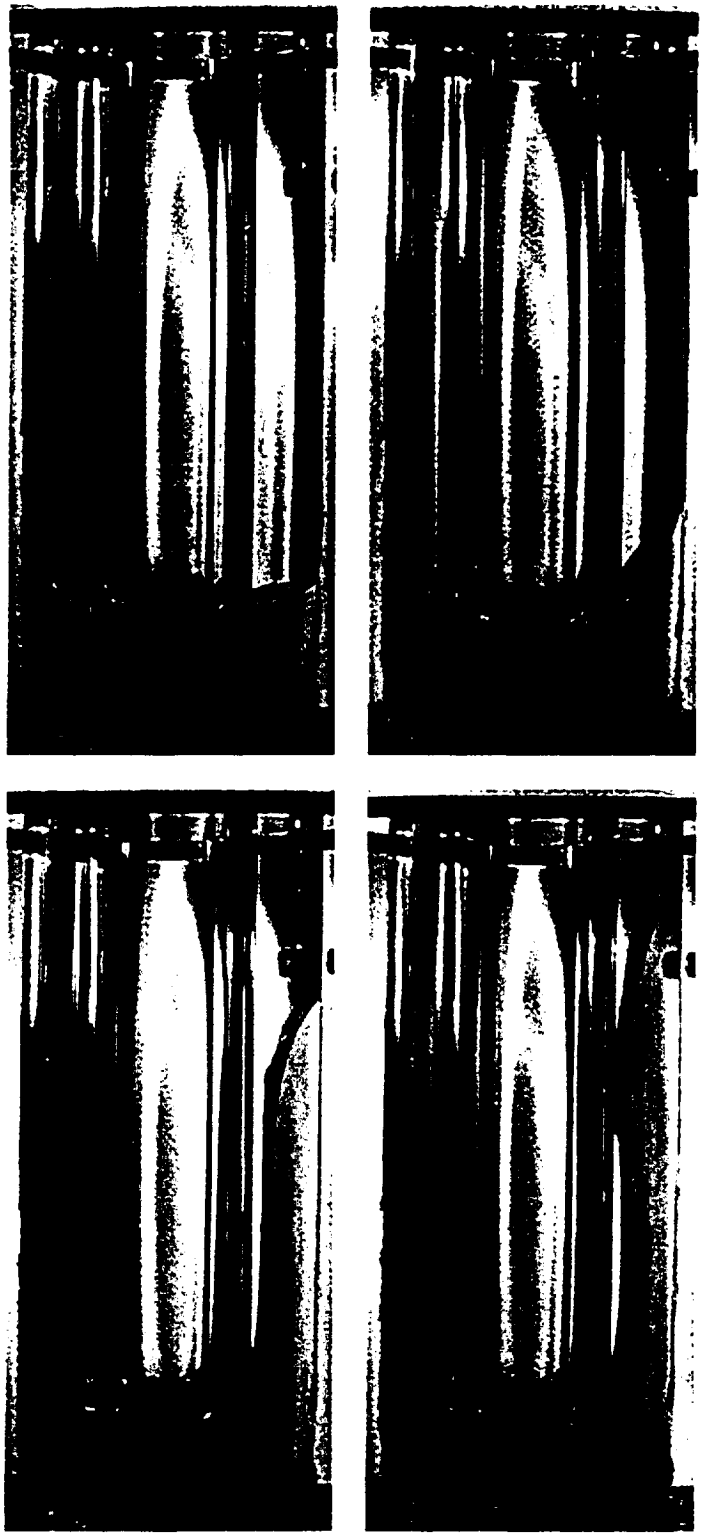

Fig 8

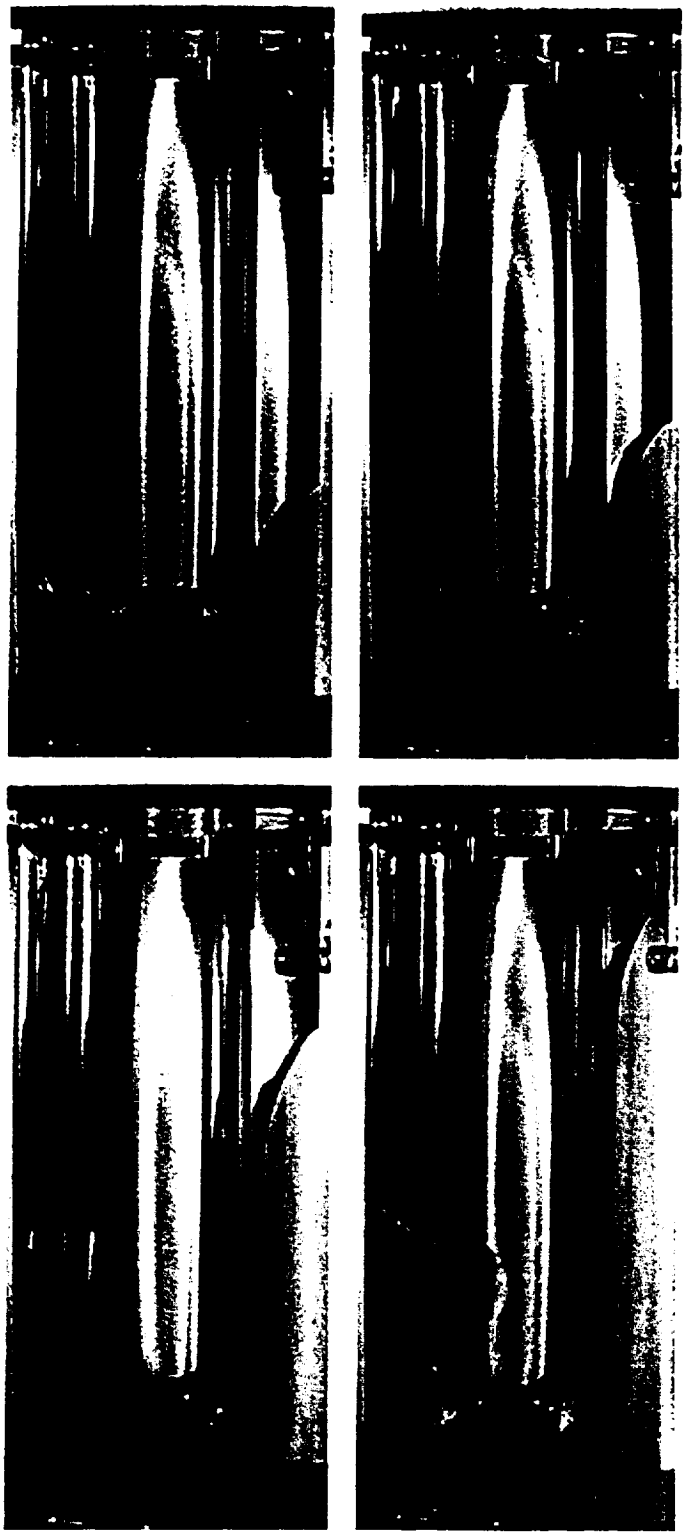

Fig 9

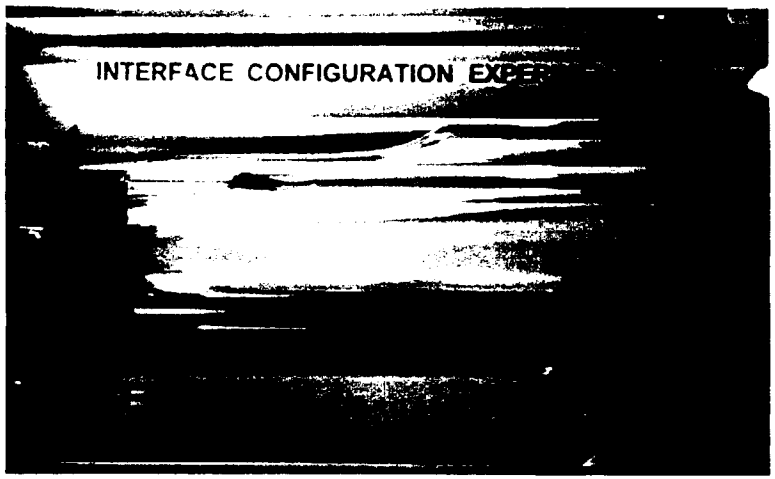

Fig 10